Comparison of control oriented models for the Long-Stator Linear Synchronous Motor and their experimental validation

R. Leidhold*, R. Benavides* and P. Mutschler*
* Darmstadt University of Technology, 64283 Darmstadt, Germany
(rleidhold@ieee.org)

***Abstract*-- In this paper, two control-oriented models for the Long-Stator Linear Synchronous Motor are presented. One of them is based on lookup tables, generated offline by Finite Element Analysis. The other one is based on the Magnetic Equivalent Circuit Method. Both models are derived from the motor geometry, magnetic characteristics of the involved materials, and the winding arrangement. Force ripple due to non-sinusoidal Electromotive Force (EMF), cogging forces and non-periodic characteristics of long stator linear motors are well simulated with these models. The intended application for these models is the design or improvement of the controllers, mainly for ripple force compensation. Results of both models were validated experimentally.**

***Index Terms*-- Linear Motors, PM Synchronous Motors, Finite Element Method, Magnetic Equivalent Circuit.**

I. Introduction

Linear Drives are becoming of increasing attention for the industry. Over the alternative of using a rotative drive with a rotative-to-linear transmission, they present advantages that include: high repeatability, low backslash, high efficiency, high dynamic response, high speed and low maintenance needs [1]. Although it is long since Linear Motors are known [2][3] it had not been of major interest for the industry, mainly because of the difficulty and high cost of driving and controlling it. It is only recently that instances of application are found due to the advances in power electronics, signal processing and control systems.

One key for designing a control system for Linear Drives is to have an adequate model, however there are no so many control-oriented models proposed as for rotative motors. In this paper, two approaches are presented for modeling a Long-Stator Linear Synchronous Motor and are compared with experimental tests results.

The first approach is based on lookup tables for implementation of the flux and force functions, which are required for the dynamic equations [4][5]. These tables are offline created by using the Finite Elements Method (FEM). It can be found several proposals of this approach for modeling Switched Reluctance Motors [5][6] demonstrating it capability for representing nonlinear characteristics. The second approach is based on the Magnetic Equivalent Circuit (MEC) method [7], which allow online computation of the flux and force values required for the dynamic equations. A model of a Short-Stator Linear motor is proposed in [8] by this approach, considering however an ideal sinusoidal flux distribution.

The resulting models are usually oriented for the controller design and simulation, e.g. for the current controller [9], or for motor drive simulation [4] (a rotative motor in this case). The models proposed in this paper include characteristics such as non-sinusoidal Electromotive Force (EMF), cogging forces and non-periodic characteristics of linear motors, providing a mean for compensating the perturbations introduced by them.

II. Motor Description

The Long-Stator Linear Synchronous Motor under study is arranged in multiple segments i.e. stators. Each segment is composed by two facing stator-sides forming a slot between them where the mover translates. An outline of one segment is shown in Fig. 1. Each segment is driven by an individual inverter. As can be appreciated in Fig. 1 each segment is curved in order to build a closed circular path. A circular path simplifies tests implementation because constant speed can be hold and rotative machines can be used for loading purposes [10].

In order to simplify the modeling, the stator is unrolled. A diagram of the unrolled stator-side and the mover is shown in Fig. 2. In the same figure, winding arrangement is also shown, which forms a three-phase system.

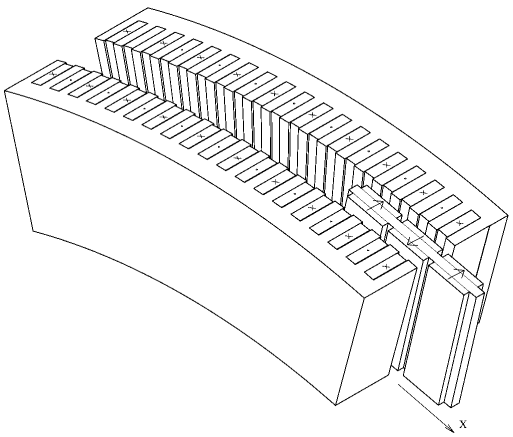

Fig. 1 Outline of one segment of the Linear Synchronous Motor

1-4244-0194-1/06/$20.00 ©2006 IEEE

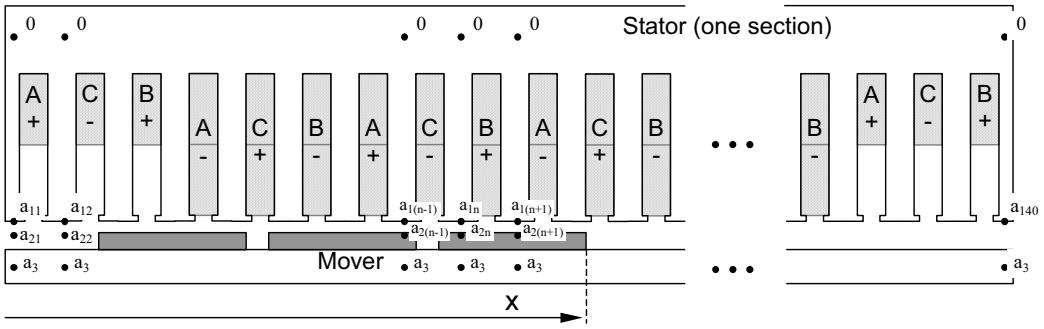

Fig. 2 Diagram of the Linear Synchronous Motor Geometry

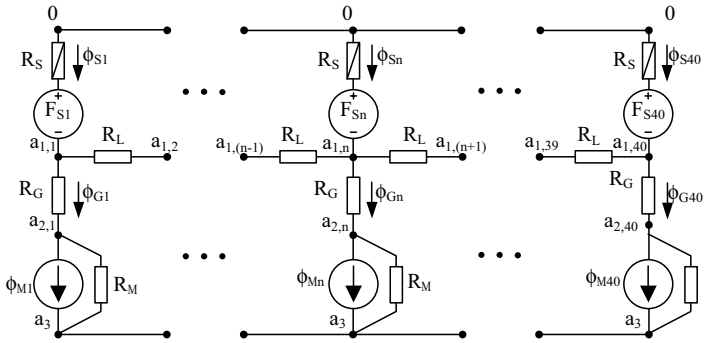

Fig. 3 Magnetic Equivalent Circuit of the Linear Synchronous Motor of Fig. 2

III. Model based on the Magnetic Equivalent Circuit

The MEC method consists in dividing the magnetic system in pieces, in which the flux flows in (almost) one direction [7]. These pieces, also called "flux tubes", are represented in the Equivalent Circuit by resistances, characterizing the magnetic reluctance (or permeance). Windings are represented in the equivalent circuit by Magneto-Motive-Force (MMF) sources. While Permanent Magnets (PM) are represented by flux sources.

Based on one unrolled stator-side of Fig. 2, the simplified Magnetic Equivalent Circuit of Fig. 3 is proposed. By it means the relation among stator MMF, stator flux and mover position can be found out. Fluxes are designated by ϕ, magneto-motive-forces by F, reluctances by R (permeances by g) and the Magnetic Potential at node $\{i,j\}$ by a_{ij}. The magnetic potential at each node in Fig. 3 is related to the corresponding points shown in the diagram of Fig. 2. Subscripts S, L, and M relates a variable or parameter to the stator, leakage and magnets respectively.

Unlike proposed by [7], where each stator's node a_{1n} would be connected with all the mover's nodes a_{2n} by position-dependent reluctances, here a simpler approach is be used. It consists on using constant airgap reluctances and position dependent flux sources. These flux sources represent the magnet area facing each stator tooth. This approach is however only possible for non-salient PM machines.

Reluctances of the leakage path R_L, the airgap R_G and the magnets R_M, are linear. Only the stator tooth reluctance R_S is considered inherently nonlinear, as there is where the flux density is higher. Because of the wide yokes, they are considered with zero reluctance.

In order to solve the MEC, the corresponding node and potential equations are derived (its derivation can be found in the Appendix I) and expressed as an implicit function:

$$0 = \mathbf{f}_1\left(\mathbf{F_S}, \mathrm{a}_3, \boldsymbol{\varphi}_\mathbf{S}, \boldsymbol{\varphi}_\mathbf{M}\right) \tag{1}$$

Where matrix and vectors are designated by bold symbols, $\boldsymbol{\varphi}_\mathbf{S} = \left[\phi_{S1} \cdots \phi_{S39}\right]$ is the stator tooth flux vector, and $\mathbf{F_S} = \left[F_{S1} \cdots F_{S39}\right]$ is the tooth MMF vector.

The magnet's flux vector $\boldsymbol{\varphi}_\mathbf{M} = \left[\phi_{M1} \cdots \phi_{M40}\right]$ is a function of the position x and is derived next. The magnet flux on the area facing the tooth-1, due to magnet-1, can be approximated by:

$$\phi_M(x) = B_r \, l_S \, b_G(x) \tag{2}$$

Where l_S is the stack length, B_r is the magnet flux density, and $b_G(x)$ is the length covered simultaneously by tooth-1 and magnet-1. The function $b_G(x)$ is implemented by a spline interpolation from the points shown in Fig. 4, where b_S and b_M are the tooth and magnet width respectively. In the same figure, the resulting curve is shown with dashed line.

The magnet flux on the area facing the nth tooth, due to the three magnets is calculates as:

$$\phi_{Mn} = \phi_M(x - x_{Tn}) - \phi_M(x - x_{Tn} - \tau_P) + \phi_M(x - x_{Tn} - 2\tau_P), \tag{3}$$

being x_{T1} the distance to the n[th] tooth and τ the pole pitch.

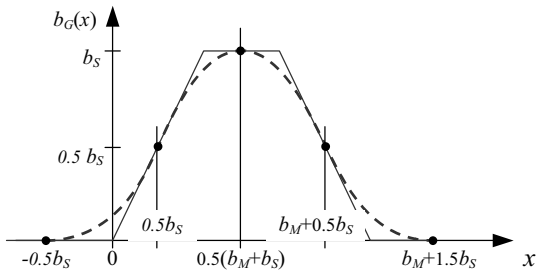

Fig. 4 Function $b_G(x)$ (airgap length covered simultaneously by one tooth and one magnet)

In order to interface the MEC with electric variables, the teeth MMF vector $\mathbf{F_S}$ is related with the phase currents as follows:

$$\mathbf{F_S} = \mathbf{w''}\,\mathbf{i} \tag{4}$$

where $\mathbf{i} = [i_A \;\; i_B \;\; i_C]^T$ is the phase current vector, and $\mathbf{w''_S}$ is the MMF transformation matrix, which can be derived from the winding distribution [7]. Similarly, the flux linkage can be related with the teeth flux vector $\boldsymbol{\varphi}_\mathbf{S}$ by:

$$\boldsymbol{\lambda} = \mathbf{w''^T}\,\boldsymbol{\varphi}_\mathbf{S} \tag{5}$$

where $\boldsymbol{\lambda}_\mathbf{S} = [\lambda_A \;\; \lambda_B \;\; \lambda_C]^T$ is the phase flux linkage vector.

By including equations (4) and (5) into (1), the MEC implicit equation becomes:

$$0 = \mathbf{f}_2(\mathbf{i}, \mathrm{a}_3, \boldsymbol{\lambda}, \boldsymbol{\varphi}_\mathbf{M}) \tag{6}$$

Once established the relation between flux and current, i.e. the magnetostatic system, it can be included in the dynamic equations. The electrical dynamic equation, with flux as state variable, is:

$$\frac{d\boldsymbol{\lambda}}{dt} = -R\,\mathbf{i} + \mathbf{u} \tag{7}$$

where $\mathbf{u} = [u_A \;\; u_B \;\; u_C]^T$ is the stator voltage vector.

The state equations are completed with the mechanical dynamics:

$$\frac{dx}{dt} = v \tag{8}$$

$$\frac{dv}{dt} = \frac{1}{M}(f - Bv - f_L) \tag{9}$$

where v is the linear speed, M is the mover's mass, B is the friction coefficient and f_L is the load force. The electromagnetic force f is calculated by the Virtual Work principle:

$$f = -\sum_n \left.\frac{dW_n}{dx}\right|_{F_n} \tag{10}$$

with W_n the magnetic energy and F_n the MMF of each element on the MEC. Because only the magnet flux vector is position dependent, the energy can be calculated as $W_n = (\mathrm{a}_{2n} - \mathrm{a}_3)\,\phi_{Mn}$. The force expression becomes:

$$f = (\mathbf{u}_2 - u_3 \mathbf{1}_{\mathbf{40x1}})^T \frac{d\boldsymbol{\varphi}_M}{dx} \tag{11}$$

where $\mathbf{1}_{\mathbf{40x1}}$ is a 40x1 matrix of ones.

The implicit nonlinear algebraic equation (6) cannot be analytically solved in order to insert it in the differential equation (7)-(9), i.e. cannot be expressed as $\mathbf{i} = \mathbf{f}(\boldsymbol{\lambda})$. Consequently, it must be solved numerically together with the differential equation.

Equations (6)-(9) form a set of differential algebraic equations (DAE). To solve the DAE, the algorithm presented in [11] is used. Otherwise, equation (6) can be solved once for each integration step of (7)-(9) using a nonlinear algebraic solver.

In the case that all reluctances are linear, equation (6) can be offline solved to be expressed as:

$$\boldsymbol{\lambda} = \mathbf{L}\,\mathbf{i} + \mathbf{M}\,\boldsymbol{\varphi}_\mathbf{M} \tag{12}$$

being $\mathbf{L}$ and $\mathbf{M}$ constant matrices.

Following, some results of the proposed method are shown. The linear motor is driven with a field-oriented scheme. The stator current is then fed with:

$$\mathbf{i} = \begin{bmatrix} \sin(x\pi/\tau) & \cos(x\pi/\tau) \\ \sin(x\pi/\tau - \tfrac{2}{3}\pi) & \cos(x\pi/\tau - \tfrac{2}{3}\pi) \\ \sin(x\pi/\tau + \tfrac{2}{3}\pi) & \cos(x\pi/\tau + \tfrac{2}{3}\pi) \end{bmatrix} \begin{bmatrix} i_d \\ i_q \end{bmatrix} \tag{13}$$

In Fig. 5, the force resulting from feeding the motor with a constant quadrature-current $i_q = 40\mathrm{A}$ and a direct-current $i_d = 0$ is shown. In this figure, the position span covers one complete segment and part of the adjacent ones, while the three segments are driven with the same current. An important force ripple can be appreciated, which is caused by the non-sinusoidal flux distribution as well as by the cogging force. The force ripple has the period of the tooth pitch (10mm). Additionally, a force reduction can be seen when the mover passes over a segment transition. This force reduction is related with the lower winding density in the first and last three slots as can be seen in Fig. 2. Also in Fig. 5, the force for zero current ($i_q = 0$), which is the cogging force, is shown. This force can be seen with more detail in Fig. 6.

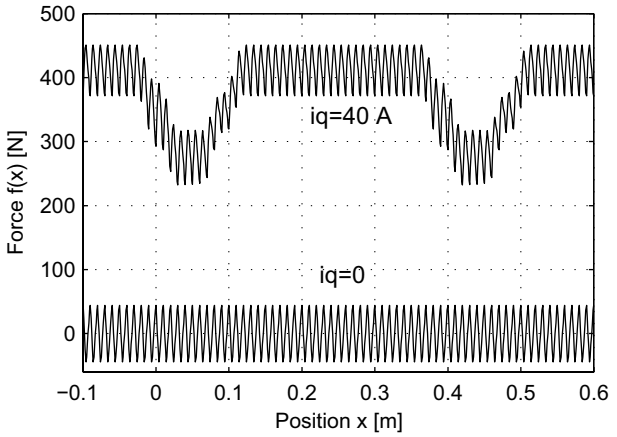

Fig. 5 Force as function of the position for $i_q = 40\mathrm{A}$ and for $i_q = 0\mathrm{A}$, obtained by the MEC based model.

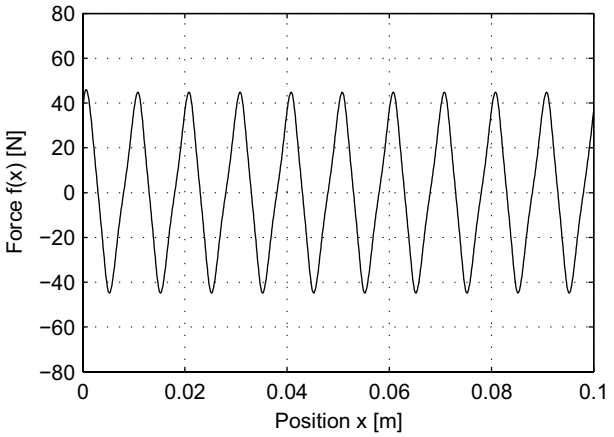

Fig. 6 Force for i_q=0A , obtained by the MEC based model.

IV. Model based on the Finite Element Method

This approach is based on using lookup tables for implementation of the nonlinear algebraic functions. When current is used as state variable for the dynamic equation, the flux derivatives functions and the force functions are required. The tables for implementing these functions are offline created by using the Finite Elements Method (FEM). The magnetostatic FEM is implemented considering nonlinear magnetic characteristics.

Flux derivative is first calculated in order to express the dynamic equation (7) with the current as state variable,

$$\frac{d\boldsymbol{\lambda}(\mathbf{i},x)}{dt}=\frac{d\boldsymbol{\lambda}(\mathbf{i},x)}{d\mathbf{i}}\frac{d\mathbf{i}}{dt}+\frac{d\boldsymbol{\lambda}(\mathbf{i},x)}{dx}\frac{dx}{dt} \tag{14}$$

Substituting (14) into (7) yields,

$$\frac{d\boldsymbol{\lambda}(\mathbf{i},x)}{d\mathbf{i}}\frac{d\mathbf{i}}{dt}=-R\,\mathbf{i}-\frac{d\boldsymbol{\lambda}(\mathbf{i},x)}{dx}v+\mathbf{u} \tag{15}$$

Where the flux derivative with respect to the current is a symmetric 2x2 matrix (in $\alpha\beta$ variables), and is a function of the current vector and the position,

$$\frac{d\boldsymbol{\lambda}(\mathbf{i},x)}{d\mathbf{i}}=\mathbf{T}_1(\mathbf{i},x)=\begin{bmatrix}T_{1\alpha\alpha}(\mathbf{i},x) & T_{1\alpha\beta}(\mathbf{i},x)\\ T_{1\beta\alpha}(\mathbf{i},x) & T_{1\beta\beta}(\mathbf{i},x)\end{bmatrix} \tag{16}$$

As the variation of the inductance depending on the position is negligible, the flux derivative with respect to the position becomes independent of the current,

$$\frac{d\boldsymbol{\lambda}(\mathbf{i},x)}{dx}=\frac{d\boldsymbol{\lambda}_M(x)}{dx} \tag{17}$$

It is a 2 elements vector (in $\alpha\beta$ variables),

$$\frac{d\boldsymbol{\lambda}_M(x)}{dx}=\mathbf{T}_2(x)=\begin{bmatrix}T_{2\alpha}(x) & T_{2\beta}(x)\end{bmatrix}^T \tag{18}$$

Finally, the force function required for the mechanical equations (8)-(9) is a scalar function, as shown,

$$f(\mathbf{i},x)=T_3(\mathbf{i},x) \tag{19}$$

In order to implement the model for a simulation, the state equations are (15), (8) and (9). Functions $\mathbf{T}_1(\mathbf{i},x)$, $\mathbf{T}_2(x)$ and $T_3(\mathbf{i},x)$ are offline calculated by FEM and stored in a lookup table. An interpolation method is online implemented for reading out these tables, avoiding excessive memory usage and time-consuming offline calculation. Matrix $\mathbf{T}_1$ is symmetric and therefore only three values must be stored for each $\{i_\alpha, i_\beta, x\}$ point. For all functions, the current dependence is smoother than the position dependence. This allows a coarser grid for the current than for the position.

When compared with the MEC based model, simulations with the FEM based model require much more memory, however, the simulation time is similar. The main difference resides in the required offline computation by FEM, which took about five days for the system analyzed in this paper, using a 2GHz AMD Athlon PC.

The force as a function of the position, obtained by this method, is shown in Fig. 7. Two curves are given: one for constant quadrature current i_q=40A , and another for zero current. In Fig. 8, the cogging force is shown with more detail.

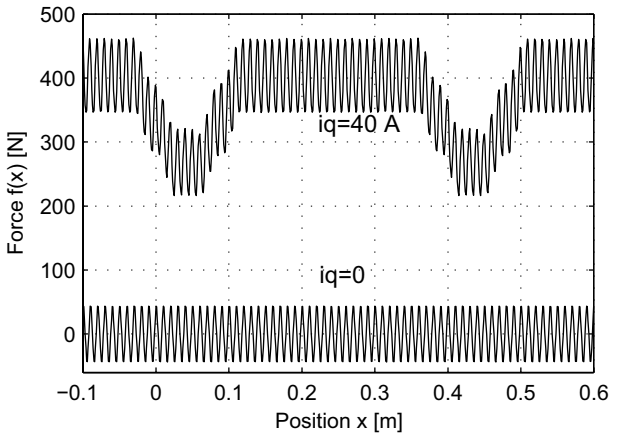

Fig. 7 Force as function of the position for i_q=40A and for i_q=0A , obtained by the FEM based model.

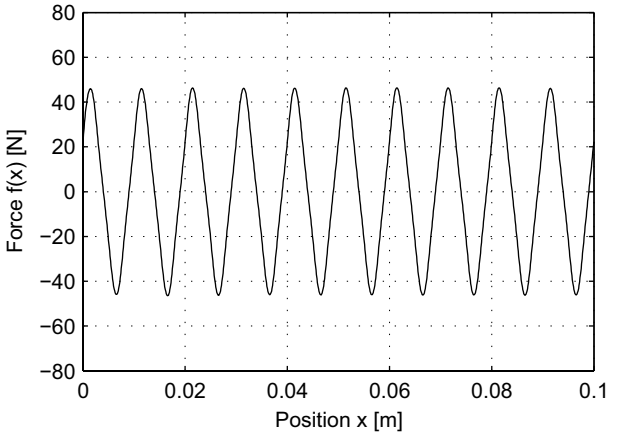

Fig. 8 Force for i_q=0A , obtained by the FEM based model.

V. Experimental Tests

Eight segments arranged in a closed circular path compose the linear PM synchronous motor. Each segment is as described in Fig. 1 and Fig. 2.

In order to experimentally measure the Linear Synchronous Motor force, it was coupled to a high torque load PM Synchronous Motor with a well-known force-current characteristic.

The force as a function of the position, obtained experimentally, is shown in Fig. 9 for quadrature current $i_q = 40A$ and $i_q = 0$. In Fig. 10, the force for zero current is presented again with another scale. Two components can be observed in the force ripple: one with the period of the tooth pitch (10mm), and another with the period of the pole pitch (30mm).

Actually, in order to allow the stator curvature, every third tooth of the stator is wedge-formed with a reduced area facing the airgap. This was not included in the model and it explains the pole-pitch component in the cogging force for the experimental results.

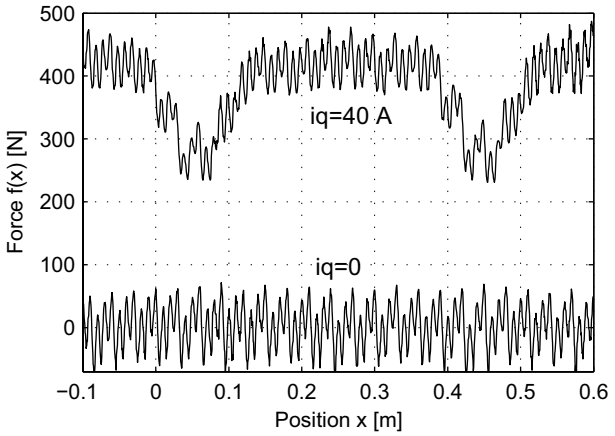

Fig. 9 Experimentally obtained a) d axis Electromagnetic Force Function, b) Fourier analysis of non current-dependent forces.

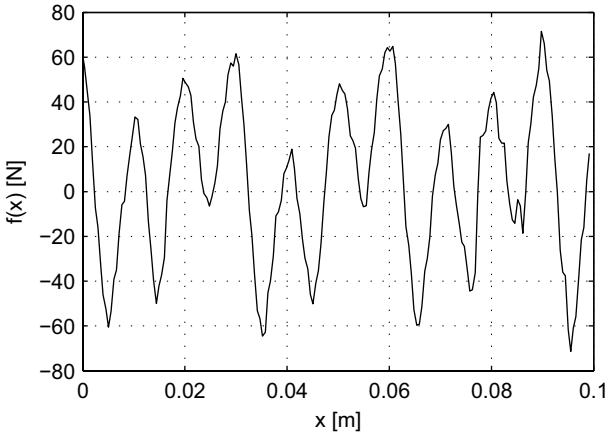

Fig. 10 Experimentally obtained a) d axis Electromagnetic Force Function, b) Fourier analysis of non current-dependent forces.

Good correspondence can be appreciated when comparing the simulation results with the experimental results, independently of which model is used. The main difference is the absence of the pole-pitch component in the modeled cogging force.

Furthermore, when comparing both simulation results, no significant difference can be found between them. This is an important achievement considering that the MEC based model is highly simplified.

VI. Conclusions

Two control-oriented models for the Long Stator Synchronous Motor were presented. One is based on the Magnetic Equivalent Circuit Method (MEC) and the other is based on lookup tables generated offline by Finite Element Method (FEM). It was shown that both models present agreement with experimental results. However, the higher agreement between both models is more remarkable.

The implementation of the FEM based model is simple and systematic. For the MEC based model, more decisions must be taken by the developer. For instance, the structure of the equivalent circuit and the function for the position-dependent flux offer some degree of freedom that can have incidences on the results.

Other important differences between both methods are the implementation and simulation times. A very long time is required for the FEM offline calculations, while simulations based on it are fast. For the MEC based model, the offline calculations as well as the simulations are very fast for linear magnetic material. For nonlinear magnetic characteristics, the simulation will become slightly slower than the FEM based. It should be considered that modifications of the model require redoing the offline calculations, which are very slow for the FEM but fast for the MEC.

Appendix I

Equations of nodes a_{0n}, a_{1n}, a_{2n}, and the equations of the teeth potentials, can be expressed in vector form, yielding respectively:

$$\mathbf{1}_{1x40}\boldsymbol{\varphi}_S = 0 \tag{20}$$

$$\boldsymbol{\varphi}_S + (g_L\mathbf{C} - g_G\mathbf{I})\mathbf{a_1} + g_G\mathbf{I}\,\mathbf{a_2} = \mathbf{0} \tag{21}$$

$$-\boldsymbol{\varphi}_M + g_G\mathbf{I}\,\mathbf{a_1} - (g_G + g_M)\mathbf{I}\,\mathbf{a}_2 + g_M\mathbf{1}_{40x1}a_3 = \mathbf{0} \tag{22}$$

$$\mathbf{a_1} + \mathbf{f}(\boldsymbol{\varphi}_S) + \mathbf{F}_S = \mathbf{0} \tag{23}$$

where $\mathbf{I}$ is the identity matrix, $\mathbf{1}_{1x40}$ is a 1x40 matrix of ones,

$$\mathbf{C} = \begin{bmatrix} -1 & 1 & 0 & \cdots & 0 & 0 & 0 \\ 1 & -2 & 1 & \cdots & 0 & 0 & 0 \\ \vdots & \vdots & \vdots & & \vdots & \vdots & \vdots \\ 0 & 0 & 0 & \cdots & 1 & -2 & 1 \\ 0 & 0 & 0 & \cdots & 0 & 1 & -1 \end{bmatrix},$$

$$\mathbf{a_1} = \begin{bmatrix} a_{1,1} \cdots a_{1,40} \end{bmatrix},$$

$$\mathbf{a_2} = \begin{bmatrix} a_{2,1} \cdots a_{2,40} \end{bmatrix},$$

and $\mathbf{f}$ is the elementwise function that relates tooth flux with its magnetic potential drop. Usually the magnetization curve is provided as a B vs. H table. From this table, a spline function can be implemented:

$$H = f_{Fe}(B) \tag{24}$$

From this function, the MMF can be related with the flux as follows:

$$F = f_{Fe}\left(\phi/(l_S b_S)\right)h = f\left(\phi\right) \tag{25}$$

where l_S is the stack length, b_S is the tooth width, and h is the tooth height.

Equations (20)-(23) form the implicit function $\mathbf{f_1}$. Additional reductions can be made by solving the linear terms (20)-(22) and including it in equation (23).

In order to derive the function $\mathbf{f_2}$, equation (21) is first substituted into (23), yielding:

$$\mathbf{a_1} + \mathbf{f}\left((g_G\mathbf{I} - g_L\mathbf{C})\mathbf{a_1} - g_G\mathbf{I}\,\mathbf{a_2}\right) + \mathbf{F_S} = \mathbf{0} \tag{26}$$

By combining equation (4) into (26), and (5) with (21), the MEC implicit equation becomes:

$$\mathbf{1_{1x40}}\boldsymbol{\varphi}_\mathbf{S} = 0 \tag{27}$$

$$\boldsymbol{\lambda} + \left(g_L\mathbf{C} - g_G\mathbf{I}\right)\mathbf{a_1} + g_G\mathbf{I}\,\mathbf{a_2} = \mathbf{0} \tag{28}$$

$$-\boldsymbol{\varphi}_\mathbf{M} + g_G\mathbf{I}\,\mathbf{a_1} - \left(g_G + g_M\right)\mathbf{I}\,\mathbf{a}_2 + g_M\mathbf{1_{40x1}}\,\mathrm{a}_3 = \mathbf{0} \tag{29}$$

$$\mathbf{a_1} + \mathbf{f}(\boldsymbol{\varphi}_\mathbf{S}) + \mathbf{F_S} = \mathbf{0} \tag{30}$$

Equations (27)-(30) form the implicit function $\mathbf{f_2}$. By solving the linear terms, additional reductions can be reached.

ACKNOWLEDGMENT

This research results were attained with the assistance of the Alexander von Humboldt Foundation, Germany. The authors would like to thank for the support.

REFERENCES

[1] A. Cassat, N. Corsi, R. Moser and N. Wavre, “Direct Linear Drives: Market and Performance Status” *Proceedings of the 4th International Symposium on Linear Drives for Industry Applications (LDIA2003),* 8-10 September 2003, Birmingham, UK. pp. 1-11.

[2] E.R. Laithwaite, *Linear electric motors*, Mill & Boon, London 1971.

[3] S.A. Nasar, I. Boldea, *Linear Motion Electric Machines*, John Wiley & Sons Inc, New York, 1976.

[4] O.A. Mohammed, S. Liu, Z. Liu, "Physical modeling of PM synchronous motors for integrated coupling with Machine drives", *IEEE Transactions on Magnetics*, Vol. 41, No. 5, pp. 1628-1631, May 2005.

[5] F. Soares and P.J. Costa Branco, "Simulation of a 6/4 Switched Reluctance Motor Based on Matlab/Simulink Environment", *IEEE transactions on Aerospace and Electronic Systems*, Vol. 37, No. 3, pp. 989-1009, Jul. 2001.

[6] B.P. Loop, S.D. Sudhoff, "Switched reluctance machine model using inverse inductance characterization", *IEEE Transactions on Industry Applications*, Vol. 39, No. 3, pp. 743-751, May-June 2003.

[7] V. Ostović, *Dynamics of Saturated Electric Machines*. Springer-Verlag. New York. 1989.

[8] H. Polinder, J.G. Slootweg, M.J. Hoeijmakers and J.C. Compter, “Modeling of a Linear PM Machine Including Magnetic Saturation and End Effects: Maximum Force-to-Current Ratio”, *IEEE Transactions on Industry Applications*, Vol.39, No.6, pp. 1681-1687, Nov/Dec 2003

[9] J. Weigel, P. Mutschler, "Modelling and control of a permanent magnet linear synchronous motor featuring unbalance and saturation including cross-saturation" *IEEE 35th Annual Power Electronics Specialists Conference, (PESC 04),* 20-25 June 2004, Vol. 3, pp. 2204-2210.

[10] R. Benavides and P. Mutschler, ”Controlling a System of Linear Drives” *IEEE Power Electronics Specialists Conference (PESC 2005)*, 12-16 June 2005, Recife, Brazil, pp 1587-1593.

[11] Shampine, Lawrence; Reichelt, Mark W.; Kierzenka, Jacek A. "Solving index-1 DAEs in MATLAB and Simulink". *SIAM Rev. 41* (1999), no. 3, pp. 538-552.